PAPER • **OPEN ACCESS**

Ion dynamics in a new class of materials: nanoglassy lithium alumosilicates

To cite this article: B Stanje *et al* 2018 *Mater. Res. Express* **5** 035202

Materials Research Express

OPEN ACCESS

RECEIVED
12 January 2018

REVISED
2 March 2018

ACCEPTED FOR PUBLICATION
8 March 2018

PUBLISHED
28 March 2018

PAPER

Ion dynamics in a new class of materials: nanoglassy lithium alumosilicates

B Stanje[1], P Bottke[1,2], S Breuer[1], I Hanzu[1,3], P Heitjans[4] and M Wilkening[1,3]

[1] Institute for Chemistry and Technology of Materials, and Christian-Doppler-Laboratory for Lithium Batteries, Graz University of Technology (NAWI Graz), Stremayrgasse 9, A-8010 Graz, Austria
[2] University of Oldenburg, Institute of Chemistry (Technical Chemistry), Carl-von-Ossietzky Str. 9-11, D-26111 Oldenburg, Germany
[3] Alistore-ERI European Research Institute, Amiens, France
[4] Leibniz Universität Hannover, Institute of Physical Chemistry and Electrochemistry, and ZFM—Center for Solid State Chemistry and New Materials, Callinstraße 3-3a, D-30167 Hannover, Germany

E-mail: wilkening@tugraz.at

Keywords: ionic diffusion, conductivity, nanostructured materials, ceramics, NMR, spin-lattice relaxation

Abstract

In many cases nanocrystalline materials, prepared through high-energy ball milling, reveal enhanced ion dynamics when compared to the situation in the coarse-grained analogues. This effect, which has particularly been seen for lithium alumosilicates, has been ascribed to structural disorder, i.e., the introduction of defect sites during mechanical treatment. Much less is, however, known about ion transport in nanostructured amorphous materials, e.g., nanoglassy compounds, which are regarded as a new class of functional materials. Following earlier studies on nanoglassy lithium alumosilicates and borates, here we studied ion dynamics in nanoglassy petalite $LiAlSi_4O_{10}$. While conductivity spectroscopy unequivocally reveals that long-range ion dynamics in nanoglassy $LiAlSi_4O_{10}$ decreases upon milling, local dynamics, sensed by ^{7}Li nuclear magnetic resonance (NMR) spin-lattice relaxation, points to enhanced Li ion mobility compared to the non-treated glass. Most likely, as for nanocrystalline ceramics also for nanoglassy samples a heterogeneous structure, consisting of bulk and interfacial regions, is formed. For $LiAlSi_4O_{10}$ these interfacial regions, characterized by a higher degree of free volume, might act as hosts for spins experiencing fast longitudinal NMR relaxation. Obviously, these regions do not form a through-going network, which would allow the ions to move over long distances as quickly as in the unmilled glass.

1. Introduction

Ion transport in nanocrystalline ceramics, which were prepared by high-energy ball milling, can be quite different from that in their coarse-grained counterparts [1, 2]. This observation also holds for nanostructured metals [3]. In many cases, the introduction of defect-rich (metastable) interfacial regions through milling causes a tremendous increase of ion diffusivity [4] in nanostructured ceramics, see also figure 1(a)). The ionic conductivity at ambient conditions of nanocrystalline oxides, such as $LiNbO_3$ [5], $LiTaO_3$ [6], Li_2TiO_3 [7], $Li_2B_4O_7$ [8] or $LiAlO_2$ [9] increases by 4–6 orders of magnitude. ^{7}Li nuclear magnetic resonance (NMR) spectroscopy confirmed the change in Li dynamics seen [6, 10–12]. The effect is accompanied by a decrease of the corresponding activation energies. In general, enhanced ion transport in nanocrystalline materials has been ascribed to the introduction of defect sites and spatially extended structurally disordered interfacial regions formed during heavy mechanical treatment [1, 4, 13–15]. Usually, shaker or planetary mills are used to prepare nanocrystalline oxides [16–18], fluorides [18, 19] or sulfides [1, 20, 21].

Sufficiently long milling produces powders with nm-sized crystallites whose ionic conductivity almost reaches that of the corresponding amorphous counterpart, that is, the glassy analogue [8]. Although plenty of studies, see, e.g., [24–31], can be found in literature that deal with ion transport phenomena and diffusion mechanisms in glasses, including also NMR investigations [1, 30–38], only few [13–15] report on the change of

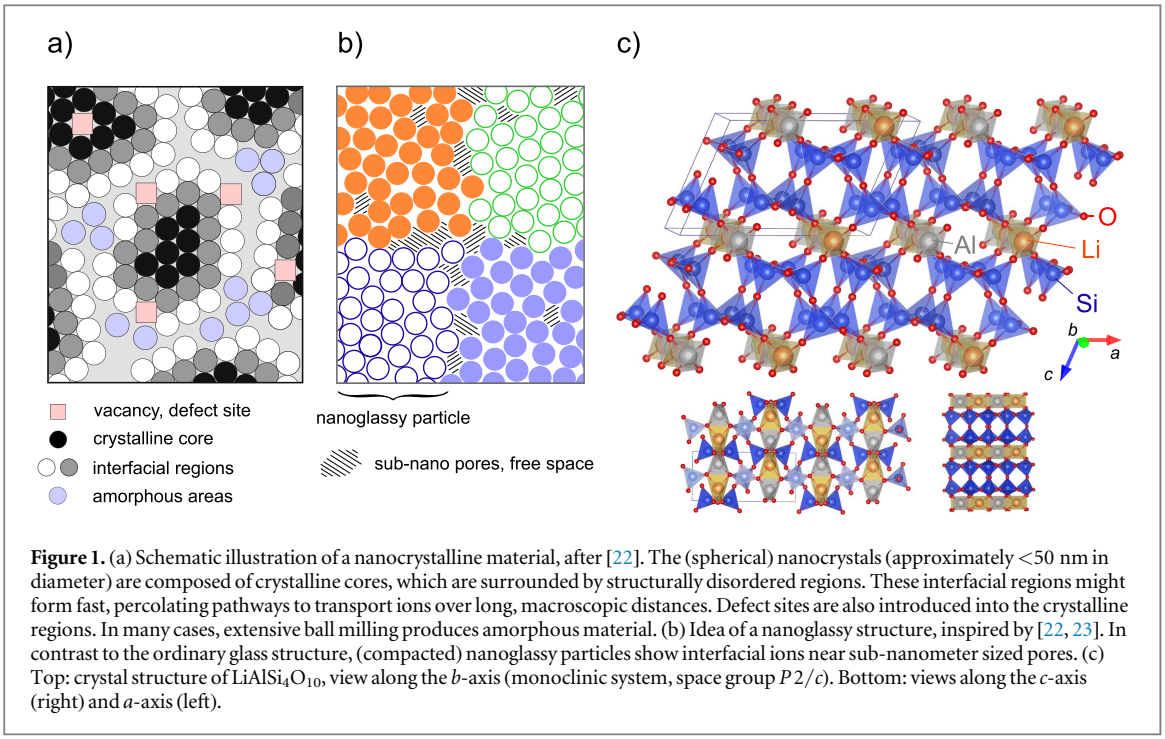

Figure 1. (a) Schematic illustration of a nanocrystalline material, after [22]. The (spherical) nanocrystals (approximately <50 nm in diameter) are composed of crystalline cores, which are surrounded by structurally disordered regions. These interfacial regions might form fast, percolating pathways to transport ions over long, macroscopic distances. Defect sites are also introduced into the crystalline regions. In many cases, extensive ball milling produces amorphous material. (b) Idea of a nanoglassy structure, inspired by [22, 23]. In contrast to the ordinary glass structure, (compacted) nanoglassy particles show interfacial ions near sub-nanometer sized pores. (c) Top: crystal structure of $LiAlSi_4O_{10}$, view along the *b*-axis (monoclinic system, space group $P2/c$). Bottom: views along the *c*-axis (right) and *a*-axis (left).

ion transport parameters if glasses were mechanically treated in high-energy ball mills. At first glance, one would expect no significant effect when an already disordered oxide is milled to form a *nanoglass* [22]. So far, two reports, however, showed that high-energy ball-milling of glassy materials, viz. $LiAlSi_2O_6$ (β-spodumene, [13, 14]) and $LiBO_2$ [14, 15] results in a decrease of the ionic conductivity. The same effect was observed for $LiAlSiO_4$ (β-eucryptite) [39]. ^{7}Li NMR line shape measurements and diffusion-induced ^{7}Li NMR spin-lattice relaxation experiments supported the findings.

For a first interpretation, a simple structural model was used to explain the observed trend [13]. The effect seen for the nanoglasses studied until now is obviously caused by a mechanically induced structural relaxation of the non-equilibrium structure of the glass, which was obtained by rapid thermal quenching [13]. Such structural relaxation is assumed to cause the ionic charge carriers to slow down with respect to those in the unmilled glass matrix. The non-relaxed glass matrix represents a state in which the mobile ions experience a higher degree of dynamic stress. Note that, referring to the Loewenstein rule [40], for β-eucryptite, for example, (local) stable and metastable forms with respect to the Al and Si ordering and coordination exist in certain temperature ranges. Ball-milling might largely influence such local and long-range arrangements of the polyhedra. Hence, the structural arrangement in a quenched glass, even in a quenched nano-glass with its metastable structural motifs [22, 23], should not necessarily be identical with that of a milled, mechanically treated sample. The latter might also exhibit a higher degree of free volume that would allow the ions, adjacent to these regions, to perform frequent jump processes (see figure 1(b)), see also [22]).

Here, we extended our earlier conductivity and NMR measurements to pétalite glass, $LiAl[Si_4O_{10}]$, a well-known lithium aluminium tectosilicate mineral. Exactly 200 years ago today, August Arfwedson, while analyzing pieces of petalite from Utö (Sweden), discovered the new element lithium (gr. λίθος, stone) [41]. Till this day it is an important ore of lithium. $LiAlSi_4O_{10}$, also known as castorite (Mohs scale hardness 6 to 6.5), crystallizes in the monoclinic system (figure 1(c)) and is a member of the feldspathoid group. Having already studied spodumene $LiAlSi_2O_6$ [13] and eucryptite $LiAlSiO_4$ [39], we are now able to compare the effect ball milling has on Li ion dynamics for three alumosilicates differing in Al:Si ratio. We will discuss similarities and differences seen by ^{7}Li NMR spin-lattice relaxometry, which is sensitive to short-range ion dynamics rather than to long-range Li ion transport. The latter, i.e., macroscopic transport, is sensed by frequency dependent, that is, alternating current, conductivity measurements in the intermediate and low frequency domains, in the following called (direct current) DC conductivities.

It is noted that the present work on petalite and the previous ones on spodumene and eucryptite (ball milled) [13–15, 39] go back to earlier systematic studies on the influence of structural disorder where we some of us compared ^{7}Li NMR spin-lattice relaxation and conductivity measurements on glasses with the compositions $Li_2O \cdot Al_2O_3 \cdot n\,SiO_2$ ($n = 2, 4, 8$) with their respective crystalline counterparts eucryptite, spodumene and petalite, still without milling [42–46]. These earlier studies showed that, at least for the alumosilicates, the Li mobility is higher in a glass than in a crystal with the same composition; for overviews we refer to [46, 47].

2. Experimental

Petalite glass specimens, $LiAlSi_4O_{10}$, were obtained in high purity from Schott Glaswerke. For comparison, we also examined glassy and crystalline $LiAlSi_2O_6$ from the same supplier. To measure the ionic conductivity of the glass samples we used a small plate (1 mm in thickness, 5 × 5 mm^2), polished the surface and applied Au electrodes (200 nm in thickness) via sputtering (Leica sputtering system). Powder samples were obtained by grinding the glass plates in an agate mortar. To prepare the various nanoglassy samples, the glass powders were milled for either 6 h or 24 h under dry conditions in ZrO_2 vials (45 ml) equipped with 180 balls (ZrO_2, 5 mm in diameter) using a Fritsch Planetary mill (Premium line 7); the ball-to-powder weight ratio was 4:1. Crystalline $LiAlSi_4O_{10}$ samples were prepared from the glassy material through devitrification at 1093 K for 300 h (heating rate 5 K min^{-1}; cooling rate 3 K min^{-1}). Crystalline $LiAlSi_2O_6$ was prepared according to the procedure described in [13]. The crystallinity of the samples was checked by x-ray diffractometry (Bruker D8 Advance, Bragg Brentano geometry); the pattern are shown elsewhere [13]. Nanocrystalline samples were prepared through ball milling under the same conditions as described for the nanoglassy samples. Alternatively, we ground up a petalite gemstone of natural origin and treated the powder in the same planetary mill for another 6 h.

To analyze complex conductivities, the powders were uniaxially cold-pressed to pellets (8 mm in diameter, 0.5 to 1 mm in thickness). After applying conducting Au electrodes, a Novocontrol Concept 80 broadband analyzer was employed to record conductivity isotherms; the frequency was varied from 0.1 Hz to 10 MHz. The isotherms revealed distinct frequency-independent plateaus from which DC conductivities σ_{DC} (see above) were read off as a function of temperature T.

^{7}Li NMR lines and relaxation rates were recorded using a Bruker Avance 500 NMR spectrometer, which was connected to a shimmed cryomagnet with a nominal field of 11 Tesla, which results in a ^{7}Li resonance frequency of 194 MHz. The probe heads (Bruker, Teflon sample chamber) used for static experiments were equipped with a type-T thermocouple connected to a Eurotherm controller to regulate the temperature with an accuracy of ±2 K. To reach temperatures above ambient we used heated nitrogen gas, for temperatures below 298 K, a stream of freshly evaporated nitrogen was employed, which was heated inside the probe. ^{7}Li NMR pulse length (90°) ranged from 2 to 3 μs depending on temperature. The well-known saturation recovery pulse sequence was used to measure longitudinal relaxation as a function of variable delay times, see [48–50] for details of this type of measurement in our laboratory. We used a comb of ten 90° pulses to destroy any longitudinal magnetization $M(t_w)$ and recorded the increase of M with a 90° detection pulse after variable delay times t_w. Up to 64 scans were accumulated per delay time. The magnetization curves were parameterized with either single or stretched exponentials to extract the rate $1/T_1$ [50]. For the analogous rotating-frame spin-lattice relaxation experiments, carried out with a nominal locking frequency of 20 kHz, we varied the locking magnetic field B_1 and approximated the transient $M_{xy}(t_{lock})$ curve with stretched exponentials, see [49, 50] for details of analogous measurement on other Li ion conductors.

3. Results and discussion

High-energy ball milling of polycrystalline samples of petalite $LiAlSi_4O_{10}$ for 6 h causes, as expected, the ionic conductivity and diffusivity to greatly increase. In figure 2(a)) the DC conductivities of micro- and nanocrystalline $LiAlSi_4O_{10}$ are shown. Considering data recorded at 360 K mechanical treatment in a planetary mill leads to an increase of the ionic conductivity by almost two orders of magnitude. Compared to, for example, $LiTaO_3$ or $LiNbO_3$ [5, 6], the change in conductivity after mechanical treatment is, however, less pronounced as crystalline $LiAlSi_4O_{10}$ shows a higher ionic conductivity from the beginning. Milling for 24 h does not change the conductivity much further. Milling the $LiAlSi_4O_{10}$ gemstone results in similar conductivity values, see dotted line in figure 2(a)).

Starting with micro-$LiAlSi_4O_{10}$ the activation energy decreased from 0.95 eV to 0.82 eV (6 h). The activation energy of the sample obtained after a milling period of 24 h is *ca.* 0.85 eV revealing a slight increase in E_a. While the sample milled for 6 h shows broadened x-ray reflections of crystalline $LiAlSi_4O_{10}$, the sample treated for 24 h is almost x-ray amorphous. Obviously, the enhancements seen originate from the structurally disordered (amorphous) regions in nanocrystalline $LiAlSi_4O_{10}$ (see figure 1(a)). A similar effect has recently been described for $Li_2B_4O_7$ [8].

Most importantly, the *opposite* trend is found when the glass is treated for several hours in the same mill. The Li ion conductivity of the glassy form significantly decreases with increasing milling. The activation energy E_a, on the other hand, has increased after the milling procedure. Initially, the glass, whose ion conductivity exceeds that of the microcrystalline form by 4 orders of magnitude (360 K), is characterized by 0.73 eV. Interestingly, $\sigma_{DC}T = f(1/T)$ of glassy $LiAlSi_4O_{10}$ resembles that of nanocrystalline $LiTaO_3$ and glassy $Li_2B_4O_7$. While

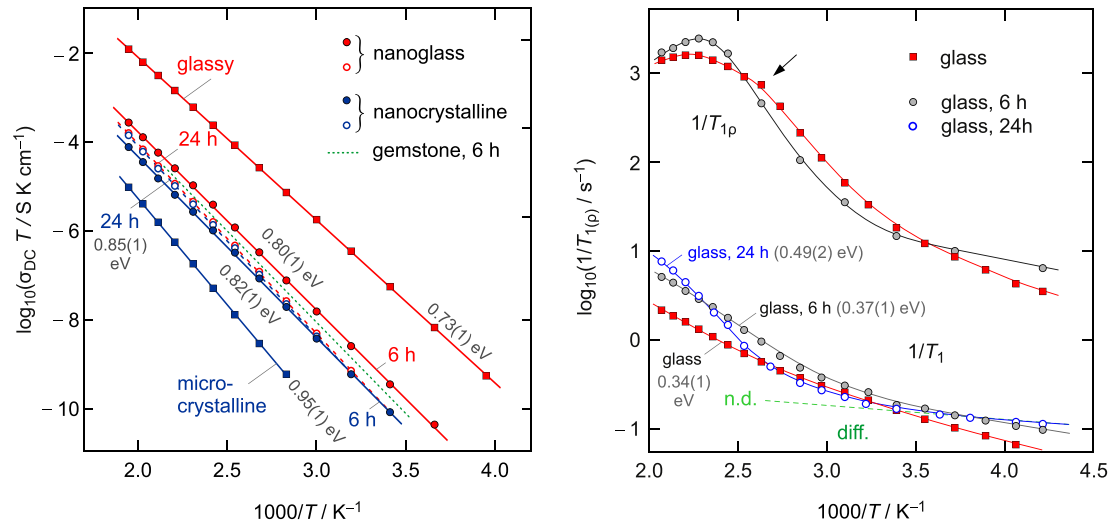

Figure 2. (a) DC conductivities of glassy and microcrystalline $LiAlSi_4O_{10}$. As expected, the ion conductivities of the glass (small plate) and the crystalline sample differ by several orders of magnitude. Milling the two materials for 6 h in a planetary mill changes the transport parameters significantly. After the milling process the conductivities headed toward each other and the activation energies converge reaching *ca.* 0.80 eV. If the milling time is further increased to 24 h the conductivities finally coincide and are governed by an activation energy of 0.85 eV. (b) ^{7}Li NMR SLR rates recorded in both the laboratory and rotating-frame of reference (Larmor frequency 194 MHz, locking frequency 20 kHz); the NMR response of the unmilled glass is compared to those of the samples that were milled for 6 h and 24 h, respectively. The solid lines are to guide the eye; n.d. denotes non-diffusive relaxation, diff. means diffusion-induced contribution. See text for further explanations.

nanoglassy $LiAlSi_4O_{10}$ (6 h) has to be characterized by $E_a = 0.80$ eV, milling the glassy oxide for another 24 h leads to a further increase and E_a reaches *ca.* 0.84 eV. The final σ_{DC} values almost coincide with those of *nanocrystalline* $LiAlSi_4O_{10}$ treated for the same period of time (approximately 0.85 eV, see above). We anticipate that the significant decrease in σ_{DC}, seen after milling for 6 h, also originates from a decreasing number density of charge carriers. Obviously, in the milled glass less ions participate in long-range ionic transport; the pre-factor of the two Arrhenius lines for the nanoglassy samples (0 h, 6 h) shown in figure 2(a) differs by one order of magnitude.

The changes in long-range ion transport, as recognized via conductivity spectroscopy, are also qualitatively seen in ^{7}Li NMR line width measurements (see [13] for very similar results) as well as in rotating-frame ^{7}Li NMR spin-lattice relaxometry (figure 2(b)). Here, such $1/T_{1\rho}$ NMR measurements have been carried out for the first time to elucidate the changes in ion dynamics of a nanoglassy material. Usually ^{7}Li NMR spin-lattice relaxation measurements are carried out at Larmor frequencies in the MHz range. These probe short-range ion dynamics as far as the corresponding NMR rates have not passed through the diffusion-induced relaxation rate peak of a log $1/T_1$ versus $1/T$ plot. The spin-lock $1/T_{1\rho}$ technique, on the other hand, takes advantage of effective locking frequencies $\omega_1/2\pi$ in the kHz range, and allows for the measurement of long-range ion diffusivities. Hence, results from $1/T_{1\rho}$ measurements are more comparable to those from DC conductivity spectroscopy than laboratory-frame $1/T_1$ measurements [46].

As compared to conductivity spectroscopy, NMR is a contactless method and no post-treatment of the samples to prepare dense pellets with conducting electrodes is needed. For a reliable description of the nanoglass effect observed here it is important to have a method at hand whose results remain unaffected by the porosity and density of the pressed pellets. Impedance or conductivity spectroscopy, in contrast to NMR, may easily suffer from careless sample preparation. Note that in figure 2, except for the glass, data of powder samples are shown.

Originally, the diffusion-induced $1/T_{1\rho}$ rates of glassy $LiAlSi_4O_{10}$ pass through a broad rate peak which seems to be composed of at least two separate peaks. One of them is indicated by the small arrow in figure 2(b). While this peak is located at 400 K, another one, the main peak, shows up at 440 K. As expected from conductivity measurements, mechanical treatment shifts the beginning of the low-T flank of the overall peak toward higher temperature. This shift unequivocally reflects a decrease in Li ion diffusivity. The higher the temperature T_{max} at which the peak appears the lower the Li diffusivity. At T_{max} the motional correlation rate, which is in simple cases within a factor of 2 directly comparable to the jump rate of the ion, is given by the angular Larmor or locking frequency, $1/\tau \approx 2\omega_1$. With $\omega_1 = 20$ kHz $\times$ 2π we obtain $1/\tau \approx 2.5 \times 10^5$ s^{-1} at

440 K, i.e., the mean residence time of a Li ion reaches values in the order of μs. At 440 K the sample milled for 6 h is characterized by an ionic conductivity in the order of 4×10^{-8} S cm^{-1}.

In addition to the shift of the NMR rate peak of the sample milled for 6 h, also the shape of the peak has changed after milling. The slope in the low-temperature range of the peak of nanoglassy $LiAlSi_4O_{10}$ is steeper than that of the glass sample. The corresponding activation energy increased from ca. 0.50 eV to 0.65 eV. Since NMR and conductivity spectroscopy, in general, probe different motional correlation functions [46, 51], one should not expect to obtain the same activation energies even though $1/T_{1\rho}$ probes ion dynamics on a comparable length scale as DC conductivity spectroscopy does. The low temperature flank of the peaks shown in figure 2(b) are additionally influenced by correlation effects such as Coulomb interactions and disorder [51], which lead to lower activation energies than expected. Here, the increase in activation energy together with the shift of the rate peak towards higher temperatures is the important difference between the two samples and overweighs the fact that not same activation energies were probed through the two methods.

Considering the change in activation energies of unmilled and milled $LiAlSi_4O_{10}$ glasses a similar behaviour, but much subtler, can be observed if we regard the ^{7}Li NMR spin-lattice relaxation rates $1/T_1$ recorded in the laboratory frame of reference (see figure 2(b)). Keeping in mind that $1/T_1$ rates are sensitive to short-range ion motions the changes after mechanical treatment might be smaller than those for σ_{DC}. While for the glass the transition from non-diffusive (n.d.) relaxation to diffusion-induced spin-lattice relaxation is almost fluent, milling causes a better separation of these regimes, see the dashed lines in figure 2(b). The increase in $1/T_1$ in the n.d.-regime might be the result of an increased number density of paramagnetic impurities introduced during milling. Alternatively, localized ion dynamics might have changed that originally caused a shallower T-dependence of the NMR rates. If we simply regard the onset of the diffusion-induced low-T flank of the $1/T_1(1/T)$ peak a shift toward higher T can be noticed, which would be in agreement with the results from both $1/T_{1\rho}$ and σ_{DC}. In agreement with this trend the associated activation energy increases from 0.34 eV for the unmilled glass to 0.37 eV for the nanoglass (6 h) and further to 0.49 eV for nanoglassy $LiAlSi_4O_{10}$, which was treated for 24 h in the planetary mill.

When interpreting these values the following needs to be considered. The relatively low value of 0.34 eV for the glass, as compared to 0.72 eV from σ_{DC} measurements, is expected to be largely influenced by correlation effects that reduce the slope of the low-T flank (see above). In general, the activation energy of the low-T flank of the $1/T_1(1/T)$ peak is related to that of the high-T flank via the following equation: E_a (low-T) $= (\alpha - 1)$ E_a(high-T). Correlation effects do not influence E_a(high-T). Only for $\alpha = 2$, which represents uncorrelated motion, symmetric peaks are obtained. In our case, if we identify E_a(high-T) with E_a from σ_{DC} (0.72 eV), we obtain $\alpha = 1.5$ indicating strongly correlated motion. Therefore, directly comparing the activation energies from low-T flanks of NMR rate peaks is not as straightforward as it looks like at first glance [52]. Milling the glass might change both E_a(high-T) and α. Even if E_a(high-T) remains constant, less correlated motion, i.e., a higher α value, would lead to steeper slopes and, hence, higher activation energies E_a(low-T). On the other hand, a constant correlation parameter and an increasing value for E_a(high-T) would also result in a steeper increase of $1/T_1$ in the low-T regime. For the glass sample milled for 24 h, with E_a(high-T) $= 0.84$ eV (see above) and E_a (low-T) $= 0.49$ eV (nanoglass, 24 h) we obtain $\alpha = 1.6$. This value indicates that less correlated ion motion seems to be present in the nanoglassy, structurally relaxed form.

Another striking fact, which additionally helps interpret the relative positions of the low-T flanks shown in figure 2(b), concerns the absolute value of the $1/T_1$ rate. It is worth noting that the rates $1/T_1$ in the diffusion-induced regime of the sample milled for 24 h significantly exceed those of the glass sample (figure 2(b)). Hence, the rates reveal more effective spin-lattice relaxation in the milled sample than in the unmilled glassy form. Interestingly, the opposite trend has been observed for β-spodumene [13]. For the sample milled for 6 h, whose activation energy (0.37 eV) is very similar to that of the glass (0.34 eV), this feature points to an increased (dipolar and/or quadrupolar) coupling constant in nanoglassy $LiAlSi_4O_{10}$. However, in the case of the sample milled for 24 h, the steeper increase of the relaxation ^{7}Li NMR rate with the inverse temperature $1/T$ indicates that the corresponding peak will be passed through at lower T. Hence, from a point of view that focusses on short-range motions sensed on the low-T side of the peak, local ion dynamics in nanoglassy $LiAlSi_4O_{10}$ (24 h), at least for some of the ions, seems to be enhanced. Such fast spin ensemble has not been observed for the other two nanoglassy systems, viz. spodumene and eucryptite, studied earlier [13, 39]. Obviously, the ensemble of spins subjected to fast longitudinal relaxation, which is responsible for the relatively steep increase of the rates above 400 K (see figure 2(b)), is not able to significantly compensate for the overall decrease in long-range ion transport as we finally obtain σ_{DC}(nanocrystalline) $\approx$ σ_{DC}(nanoglassy), see the overview presented in figure 3(a).

Most likely, also for nanoglassy samples a heterogeneous structure consisting of bulk and interfacial regions is formed. For $LiAlSi_4O_{10}$ these interfacial regions, characterized by a higher degree of free volume, might act as hosts for the fast relaxing spins (see figure 1(b)). The higher E_a (0.49 eV), as compared to that of the unmilled glass sample (0.34 eV), indicates (local) Li motions less influenced by correlation effects rather than a higher

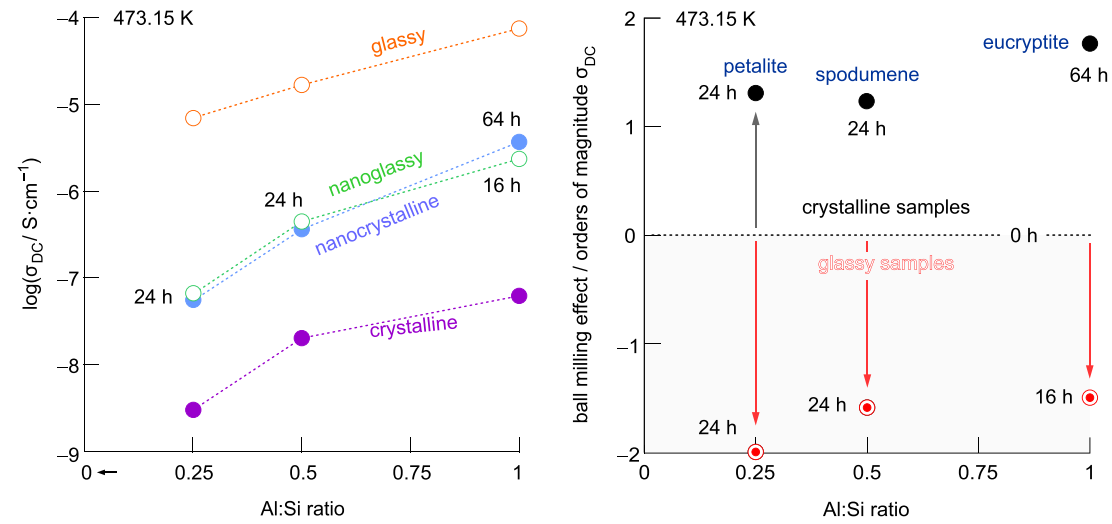

Figure 3. (a) Change in ionic conductivity, at 473.15 K, when going from crystalline to glassy lithium alumosilicates; data refer to $LiAlSiO_4$ [39], $LiAlSi_2O_6$ (this work, similar values were reported in [13]) and $LiAlSi_4O_{10}$ (this work) with Al:Si ratios of 1, 0.5 and 0.25. In all three cases σ_{DC}(nanoglassy) is lower than σ_{DC}(glassy). Data for nanoglassy and nanocrystalline samples refer to the milling times indicated. Except for β-eucryptite we obtain σ_{DC}(nanoglassy) $\approx$ σ_{DC}(nanocrystalline) revealing a very similar microstructure of the nanostructured samples. For $LiAlSiO_4$, which shows, contrary to the other alumosilicates, a slightly higher density in its glassy form, we found σ_{DC}(nanoglassy) $<$ σ_{DC}(nanocrystalline); thus, it might take a special rôle. (b) Increase or decrease of the ionic conductivity (in orders of magnitude) when crystalline or glassy samples were milled for 24 h or, in the case of eucryptite, for 64 h and 16 h, respectively. We assume that after 64 h (and 16 h) the limiting values of σ_{DC} were (already) reached. As an example, milling of crystalline $LiAlSi_4O_{10}$ (indicated by '0 h') for 24 h causes σ_{DC} to increase by almost 1.5 orders of magnitude, whilst σ_{DC} of the glassy form decreased by 2 orders of magnitude.

mean hopping barrier. Obviously, these regions do not form a through-going network to enable the ions to move over long distances as quickly as in the original glassy state obtained by quenching.

As a last remark, by comparing the effect seen in σ_{DC} for $LiAlSiO_4$ and $LiAlSi_2O_6$ we notice that the ratio $\sigma_{g:n} = \sigma_{DC}$(glassy):$\sigma_{DC}$(nanoglassy) is similar and close to 1, see figures 3(a) and (b) which gives an overview of the samples studied so far. We clearly notice that for Al:Si $= 1$ the largest decrease in ionic conductivity, viz. by ca. 2 orders of magnitude, is found when $LiAlSi_4O_{10}$ glass is milled. The fact that $\sigma_{g:n}(LiAlSiO_4) < 1$ might be related to the fact that the density of β-eucryptite glass is higher than that of the crystalline form. This observation should, however, not be overinterpreted. For $LiAlSi_4O_{10}$ we have also seen that σ_{DC} of the nanocrystalline sample prepared from the gemstone, even if only milled for 6 h, slightly exceeds that of the nanoglassy sample (milled for 24 h), see figure 2(a). Slight variations in chemical compositions and marginal impurities easily lead to such small changes in ionic conductivities.

While for $LiAlSiO_4$ and $LiAlSi_2O_6$ the $1/T_1$ NMR response points to the same direction as was observed through conductivity measurements viz to a decrease of Li ion dynamics upon milling the glassy forms, for $LiAlSi_4O_{10}$ the situation is more complex. The differences seen by ^{7}Li NMR laboratory-frame spin-lattice relaxations measurements discussed above might be connected to the lower Al content in $LiAlSi_4O_{10}$. Further NMR measurements, extending earlier ones on the glassy form [45], and particularly using the ^{7}Li SAE NMR technique, are in progress in our laboratory to throw light on the heterogeneous ion dynamics in nanoglassy $LiAlSi_4O_{10}$,

4. Summary and conclusions

Nanostructured materials are of large and ever-growing interest due to their beneficial properties. In particular, nanocrystalline ceramics find applications as catalysts, sensors, adsorbents or new electrolytes and advanced electrode materials in electrochemical energy storage. The formation of nanocrystalline ceramics via high-energy ball-milling leads to ion conductors with, in many cases, greatly improved ionic transport properties.

The increase in ionic conductivity of crystalline $LiAlSi_4O_{10}$, observed when the material is milled for several hours in a high-energy ball mill, can be explained by the formation of structurally disordered interfacial regions and the amount of amorphous material produced. It turned out that, also in the case of $LiAlSi_4O_{10}$, ion transport properties can be easily manipulated by tuning the degree of structural disorder. Importantly, mechanical treatment of the glass clearly causes the ionic conductivity to decrease, finally coinciding with that of the heavily

treated nanocrystalline, almost x-ray amorphous $LiAlSi_4O_{10}$. We explain this effect by mechanically induced structural relaxation, i.e., the release of strain and the reduction of free Gibbs energy of the glassy system upon mechanical treatment. By mechanical treatment the gap in ionic conductivity between crystalline and glassy $LiAlSi_4O_{10}$ can easily been closed and allows us to tune ionic conductivities over many orders of magnitude. For instance, the ionic conductivity at $T = 330$ K changed by a factor of 10^4.

Spin-lock ^{7}Li NMR relaxations measurements performed in the rotating frame of reference match very well with the findings from conductivity measurements. Our results from laboratory-frame ^{7}Li NMR relaxometry, however, reveal a more complex dynamic situation in nanoglassy $LiAlSi_4O_{10}$. In samples treated for a sufficiently long time in planetary mills, the Li spins have access to distinctly fast local diffusion pathways. Most likely, ions near the interfacial regions of the nanoglassy particles do take part in these NMR relaxation processes.

Acknowledgments

We thank the Deutsche Forschungsgemeinschaft for financial support (FOR 1277, Mobility of Lithium Ions in Solids, sub-project 7). Moreover, additional financial support by the Austrian Federal Ministry of Science, Research and Economy, and the Austrian National Foundation for Research, Technology and Development (in the frame of the Christian Doppler Laboratory of Lithium Batteries: Ageing Effects, Technology and New Materials) is greatly appreciated. P H is grateful to the State of Lower Saxony (Germany) for a Niedersachsen Professorship.

ORCID iDs

I Hanzu https://orcid.org/0000-0002-9260-9117
M Wilkening https://orcid.org/0000-0001-9706-4892

References

[1] Prutsch D *et al* 2017 *Z. Phys. Chem.* **231** 1361
[2] Heitjans P and Wilkening M 2009 *Defect Diffus. Forum* **283–286** 705
[3] Würschum R, Reimann K and Farber P 1997 *Defect Diffus. Forum* **143** 1463
[4] Heitjans P and Indris S 2003 *J. Phys. Condens. Matter* **15** R1257
[5] Heitjans P, Masoud M, Feldhoff A and Wilkening M 2007 *Faraday Discuss.* **134** 67
[6] Wilkening M, Epp V, Feldhoff A and Heitjans P 2008 *J. Phys. Chem.* C **112** 9291
[7] Brandstätter H, Wohlmuth D, Bottke P, Pregartner V and Wilkening M 2015 *Z. Phys. Chem.* **229** 1363
[8] Wohlmuth D, Epp V, Stanje B, Welsch A M, Behrens H and Wilkening M 2016 *J. Am. Ceram. Soc.* **99** 1687
[9] Wohlmuth D, Epp V, Bottke P, Hanzu I, Bitschnau B, Letofsky-Papst I, Kriechbaum M, Amenitsch H, Hofer F and Wilkening M 2014 *J. Mater. Chem.* A **2** 20295
[10] Wilkening M, Bork D, Indris S and Heitjans P 2002 *Phys. Chem. Chem. Phys.* **4** 3246
[11] Bork D and Heitjans P 2001 *J. Phys. Chem.* B **105** 9162
[12] Bork D and Heitjans P 1998 *J. Phys. Chem.* B **102** 7303
[13] Kuhn A, Wilkening M and Heitjans P 2009 *Solid State Ion.* **180** 302
[14] Kuhn A, Tobschall E and Heitjans P 2009 *Z. Phys. Chem.* **223** 1359
[15] Heitjans P, Tobschall E and Wilkening M 2008 *Eur. Phys. J.—Spec. Top.* **161** 97
[16] Šepelák V, Düvel A, Wilkening M, Becker K D and Heitjans P 2013 *Chem. Soc. Rev.* **42** 7507
[17] Indris S, Bork D and Heitjans P 2000 *J. Mater. Synth. Process.* **8** 245
[18] Wilkening M, Düvel A, Preishuber-Pflügl F, da Silva K, Breuer S, Šepelák V and Heitjans P 2017 *Z. Krist.-Cryst. Mater.* **232** 107
[19] Preishuber-Pflügl F and Wilkening M 2016 *Dalton. Trans.* **45** 8675
[20] Winter R and Heitjans P 2001 *J. Phys. Chem.* B **105** 6108
[21] Winter R and Heitjans P 1999 *Nanostruct. Mater.* **12** 883
[22] Gleiter H 2013 *Beilstein J. Nanotech.* **4** 517
[23] Padmanabhan K A and Gleiter H 2014 *Beilstein J. Nanotech.* **5** 1603
[24] Bunde A, Funke K and Ingram M D 1998 *Solid State Ion.* **105** 1
[25] Funke K, Roling B and Lange M 1998 *Solid State Ion.* **105** 195
[26] Ngai K L 2000 *J. Non-Cryst. Solids* **275** 7
[27] Funke K 2013 *Sci. Technol. Adv. Mat.* **14** 043502
[28] Sidebottom D L 1999 *Phys. Rev. Lett.* **83** 983
[29] Almond D P and West A R 1983 *Nature* **306** 456
[30] Böhmer R and Qi F 2007 *Solid State Nucl. Magn. Reson.* **31** 28
[31] Faske S, Koch B, Murawski S, Küchler R, Böhmer R, Melchior J and Vogel M 2011 *Phys. Rev.* B **84**
[32] Wilkening M, Kuhn A and Heitjans P 2008 *Phys. Rev.* B **78**
[33] Tang X P, Busch R, Johnson W L and Wu Y 1998 *Phys. Rev. Lett.* **81** 5358
[34] Gabriel J, Petrov O V, Kim Y, Martin S W and Vogel M 2015 *Solid State Nucl. Magn. Reson.* **70** 53
[35] Faske S, Eckert H and Vogel M 2008 *Phys. Rev.* B **77**
[36] Böhmer R, Jeffrey K R and Vogel M 2007 *Prog. Nucl. Magn. Reson. Spectrosc.* **50** 87
[37] Vogel M, Brinkmann C, Eckert H and Heuer A 2002 *Solid State Nucl. Magn. Reson.* **22** 344

[38] Vogel M, Brinkmann C, Eckert H and Heuer A 2002 *Phys. Chem. Chem. Phys.* **4** 3237
[39] Bottke P 2010 *Diploma Thesis* Leibniz University Hannover
[40] Loewenstein W 1954 *Am. Mineral.* **39** 92
[41] Arfwedson A 1818 *Journal für Chemie und Physik* **22** 93
[42] Munro B, Schrader M and Heitjans P 1992 *Ber. Bunsen-Ges. Phys. Chem. Chem. Phys.* **96** 1718
[43] Franke W and Heitjans P 1992 *Ber. Bunsen-Ges. Phys. Chem. Chem. Phys.* **96** 1674
[44] Qi F, Rier C, Böhmer R, Franke W and Heitjans P 2005 *Phys. Rev.* B **72**
[45] Winter R, Siegmund K and Heitjans P 1997 *J. Non-Cryst. Solids* **212** 215
[46] Heitjans P, Schirmer A and Indris S 2005 *Diffusion in Condensed Matter—Methods, Materials, Models* ed P Heitjans and J Kärger (Berlin: Springer) pp 367
[47] Chandran C V and Heitjans P 2016 *Ann. Rep. NMR Spectrosc.* **89** 1
[48] Epp V, Gün O, Deiseroth H J and Wilkening M 2013 *J. Phys. Chem. Lett.* **4** 2118
[49] Epp V, Gün O, Deiseroth H J and Wilkening M 2013 *Phys. Chem. Chem. Phys.* **15** 7123
[50] Epp V and Wilkening M 2015 *Handbook of Solid State Batteries* (Singapore: World Scientific) pp 133
[51] Preishuber-Pflügl F, Bottke P, Pregartner V, Bitschnau B and Wilkening M 2014 *Phys. Chem. Chem. Phys.* **16** 9580
[52] Stanje B, Epp V, Nakhal S, Lerch M and Wilkening M 2015 *ACS Appl. Mater. Interface* **7** 4089